Monthly Notices of the ROYAL ASTRONOMICAL SOCIETY

MNRAS **527,** 11082–11089 (2024) https://doi.org/10.1093/mnras/stad3937
Advance Access publication 2023 December 22

Stellar rotations and the disentanglement of the Galactic thin and thick discs

M. P. da Silva [1]★ A. Alves-Brito[2] and J. D. do Nascimento Jr.[1,3]

[1]*Departamento de Física, Universidade Federal do Rio Grande do Norte, 59072-970 Natal, RN, Brazil*
[2]*Universidade Federal do Rio Grande do Sul, Instituto de Física, Av. Bento Gonçalves 9500, Porto Alegre, RS, Brazil*
[3]*Harvard-Smithsonian Center for Astrophysics, Cambridge, MA 02138, USA*

Accepted 2023 December 19. Received 2023 December 18; in original form 2023 July 17

ABSTRACT

The kinematics, mean α-elements, and ages of the stars reveal two distinct disc populations observed in the Solar neighbourhood. Although several studies have been carried out to characterize abundances of chemical elements and kinematic identifications in these populations, there are few studies that dealt with the analysis of stellar rotation and characteristics of populations focused on low-mass stars of the F and G types. In this work, we propose a new approach to classify stellar populations from the thin and thick disc for F and G dwarf stars by relating chemical abundance and rotation ($v \sin i$) of these stars in the rotational–chemical–plane ($v \sin i$–[α/Fe]–[Fe/H] plot). Our results show that the two rotational-chemical sequences disentangled, high- and low-[α/Fe] components, present properties (α-enhanced, ages, kinematics, space velocity gradients, local density ratio) closely linked to the stars of the chemically and kinematically defined as thin and thick disc components. This study has an impact on calibrations that relate ages to rotation (gyro-chronology) as well as age to chemical abundances (chemochronology), as well as sheds light on the understanding of the processes of Galactic disc formation.

Key words: stars: fundamental parameters – stars: kinematics and dynamics – stars: rotation – Galaxy: abundances – Galaxy: disc – Galaxy: evolution.

1 INTRODUCTION

The study of stars in the Solar neighbourhood (and beyond) has revealed a number of Milky Way components, such as thin and thick discs, as well as halo stars, including the comprehension of their chemical and kinematic properties. Essentially, there are three ways to determine these stellar populations of the Galactic disc: by kinematic, chemistry, or age criteria. Due to the overlap of the thin and thick disc space velocity distributions, the 'classical method' of classifying the stars from the kinematics as belonging to one of the disc components results in greater contamination of the samples (Bensby, Feltzing & Lundström 2003). Furthermore, because of the dynamic heating caused by multiple stochastic interactions associated with giant molecular clouds (GMCs) or star clusters (Spitzer & Schwarzschild 1951, 1953), spiral arms (Sellwood & Binney 2002), and other non-axissymmetric structures, space velocity as well as position do not necessarily represent the characteristics of the star's birthplace. In contrast, the chemical abundance as a stable property closely linked to the stellar birth makes the chemical criterion more reliable; however, as is commonly used, the delimitation between thin and thick disc components from regions of low density in α-enhancement [α/Fe] versus metallicity [Fe/H] plane is somewhat arbitrary (Navarro et al. 2011; Franchini et al. 2020) or is not very clear (Bovy, Rix & Hogg 2012; Minchev, Chiappini & Martig 2013), specially at higher metallicities where the separation of stellar populations is often performed by eye or with rather fiducial straight lines as highlighted by Buder et al. (2019). In addition, the clarity of this separation criterion depends, to a large extent, on the quality of the data available for analysis (see Queiroz et al. 2023), making this type of approach challenging or unfeasible for low- and medium-resolution data (e.g. Lee et al. 2011; Wojno et al. 2016; Ho et al. 2017), and even for high-resolution samples at the metal-rich regime (e.g. Recio-Blanco et al. 2014; Buder et al. 2019; Mackereth et al. 2019a). Finally, segregating samples exclusively by age also results in contamination between different disc populations because of the wide margin of error present in the estimated ages.

Since the first observations of the apparent separation of high- and low-[α/Fe] values as a function of [Fe/H] (Fuhrmann 1998; Gratton et al. 2000; Prochaska et al. 2000), the bimodality of [α/Fe] ratios is often interpreted as the physical distinction between populations of the thin and thick disc (e.g. Adibekyan et al. 2011; Navarro et al. 2011; Recio-Blanco et al. 2014). This assumption is based on the interpretation that the [α/Fe]–[Fe/H] plane is predominantly a stellar population diagram (Fuhrmann 1998), where the discrete separation of the two sequences, high- and low-[α/Fe], possibly reflects the star formation gap between the thin and thick disc. The fact that the thick disc is enriched by [α/Fe] indicates that this population was formed early in the history of the Galaxy, when the progenitor gas was less polluted by type Ia supernovae (Type Ia SN) and enriched mainly with α-elements synthesized by type II supernovae (Type II SNe) (Kobayashi & Taylor 2023). In turn, thin disc stars being

★ E-mail: moises.psilv@gmail.com

depleted in α-elements and with considerable abundance in Fe, this indicates that they belong to a younger stellar population. Therefore, the [α/Fe] versus [Fe/H] plane presents us with two very different age sequences.

Based on what was mentioned above, with access to a suitable stellar age proxy, along with α-enhancement and metallicity, we can, in principle, disentangle the stellar components of the Galactic disc. Similarly to how the α-element abundances act as potential chemical-clocks in the dissection of stellar populations of the disc, another straightforward and simple observable-clock candidate is the angular rotation velocity of low-mass stars. But contrary to the chemical composition that can remain unchanged for billions of years in the atmosphere of dwarf stars, enabling one to obtain the chemical footprint of the gas from which they formed, the rate at which stars rotate on their own axes is a mutable observable that decreases throughout time. Stellar spin down through loss of angular momentum is a complex mechanism involving magnetism, dynamo, mass, rotation, etc. Despite the complexity of the mechanisms involved in the stellar rotation evolution, the connection of rotational velocity decrease with age may be remarkably well established on the main sequence; for low-mass stars, the behaviour of the rotation angular velocities with age follows a power law, $\Omega(t) \sim t^{-b}$ (Soderblom 1983; Kawaler 1988; Barnes 2003), where $b = 0.5$ is well-known Skumanich relation (Skumanich 1972). The origin of this relationship lies in magnetized stellar winds – where winds can drain off angular momentum – which is a dominant mechanism in Sun-like and later type stars that have a deep convective envelope, resulting in a strong coupling of rotation and magnetic activity through stellar dynamo. In this study, based on chemo- and gyro-chronology principles, we present a new method for determining the Galactic disc components from [α/Fe] and [Fe/H] abundances in combination with stellar rotation, specifically the projected rotational velocity ($v \sin i$).

2 SAMPLE SELECTION

As our core assumption of disentangling of stellar disc populations is based entirely on the distinction of stellar rotation in different regions of [α/Fe] ratios along the metallicity, in which a priori this distinction is independent of any occurrence of gap or bimodality of α-elements on the chemical plane, we use wide estimates of abundance ratios [α/Fe] obtained by Strömgren photometry from Casagrande et al. (2011) and the projected rotational velocities, $v \sin i$, from the Geneva–Copenhagen Survey (GCS) (Nordström et al. 2004; Holmberg, Nordström & Andersen 2007, 2009). The work of Casagrande et al. (2011) provides reanalysed astrophysical parameters from the GCS data such as effective temperature, mass, age, and chemical abundances for stars in the Solar neighbourhood. The estimated values of [α/Fe] obtained by these authors from the Strömgren indices are only a proxy of the real [α/Fe] abundances (see Casagrande et al. 2011, for more details). Therefore, these measurements are less accurate than those obtained by high-resolution spectroscopy, which makes it impossible to recover any gap between the disc populations, as can be seen in the [α/Fe] distribution shown in Fig. 1. None the less, according to Casagrande et al. (2011), even though estimated [α/Fe] values for thin disc stars may exhibit slight underestimations/overestimations at higher/lower metallicities, overall agreement with high-resolution spectroscopic data remains good, with an average deviation of 0.09 dex. The present sample provides a large amount of [α/Fe] ratio estimates for $\sim$ 16 000 FG(K) dwarfs, and although less accurate, the large number of stars can give us important information about the Galactic disc. We used

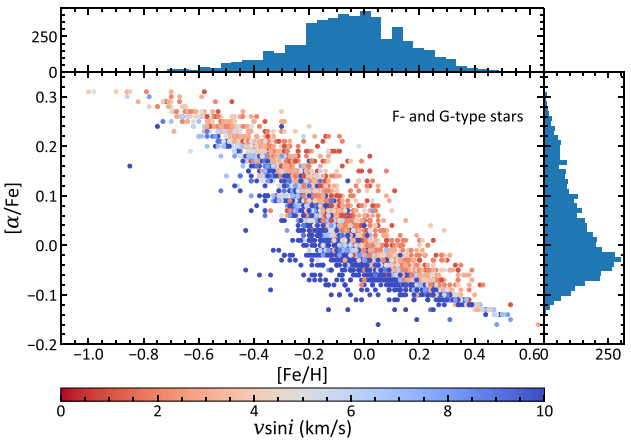

Figure 1. The [α/Fe]–[Fe/H] diagram, coloured by $v \sin i$ values. The maximum value of 10 km s^{-1} in the colour scale was conveniently chosen to highlight the distinction between the two possible populations; the values of $v \sin i$ range from 1 to 20 km s^{-1}. The panels located at the top and on the right side are histograms of the [Fe/H] and [α/Fe] ratios, respectively.

in our analysis expectations ages from BASTI isochrones of the referred work. With respect to stellar rotation, the $v \sin i$ data from the GCS were obtained from observations with the photoelectric cross-correlation spectrometers CORAVEL, with an uncertainty of about 1 km s^{-1} for stars with rotations smaller than 30 km s^{-1} (de Medeiros & Mayor 1999). The vast majority of the stars in the sample have rotations below 20 km s^{-1}.

On the α-elements over iron abundance as a function of metallicity one should expect two distinctly separate populations in young and oldest stars, but we do not see exactly this separation for 9000 age-determined stars – we exclude here and throughout the study stars from binary systems and clusters. But when we restrict the volume of our sample to 120 pc and consider only stars with $v \sin i > 0$ and temperatures greater than 5400 K (discarding abundances with greater uncertainties) we recover the expected pattern, see Fig. 1. Other works have also applied a similar cutoff to the temperature at which a greater increase in uncertainties in abundances is observed for cold stars, in general, stars with temperatures lower than 5000 to 5400 k (e.g. Adibekyan et al. 2013; Bensby, Feltzing & Oey 2014). Interestingly, in the upper plot of Fig. 1, in the rich-[α/Fe] region ([α/Fe] $\sim$ 0.16, [Fe/H] $\sim$−0.12), there are some apparently young stars (2 to 5 Gyr). However, these same stars present in this α-enhanced region have low rotation velocity, characteristics of old stars, which shows us that possibly the ages determined for these stars are underestimated or, less likely, the values of [α/Fe] are overestimated with the measurements of $v \sin i$ also incorrect. Our final sample is composed of 5129 F and G single dwarf stars.

3 DISENTANGLING THE F- AND G-TYPE STARS FROM THE THIN DISC AND THE THICK DISC

Many works have been dedicated to studying the relationship between stellar kinematics with chemical abundance and age separately. However, as seen recently in several works, chemical abundance and stellar age do not present a simple correlation, as, for example, the [α/Fe]–[Fe/H] diagram as a function of age (e.g. Haywood et al. 2016; Mackereth et al. 2019b). Given that dwarf stars like the FG(K)-types are stable objects capable of retaining their atmospheres practically intact for billions of years, the non-trivial relationship in the chemical

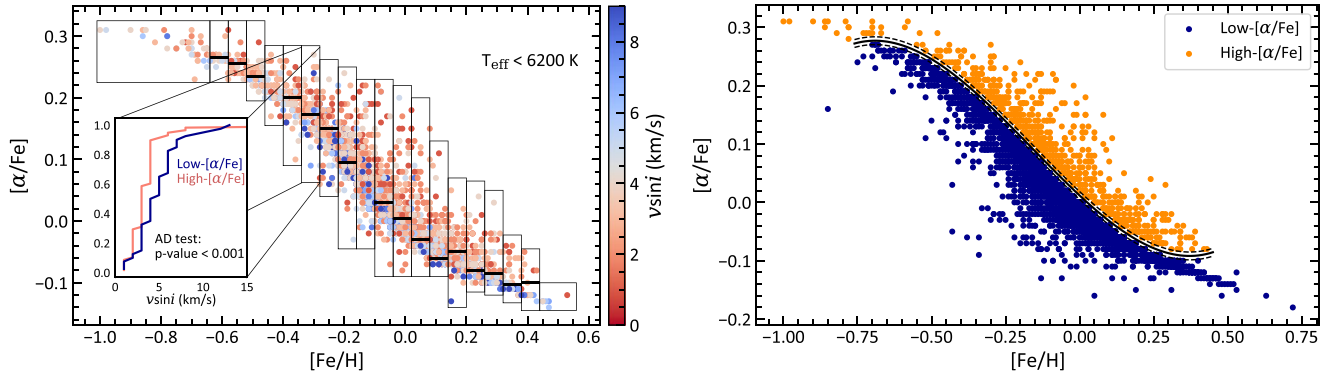

Figure 2. α-elements over iron abundance as a function of metallicity. Left panel: example of identification of [α/Fe] regions with distinct rotational distributions along the [Fe/H] ratios in ranges of 0.06 dex. Right panel: the high- and low-[α/Fe] components separated and rotational velocity curve of the chemical plane obtained by the polynomial fit of the tests, where the dotted curves are the average uncertainty (1σ) from the standard deviation from each [α/Fe] separation region found.

plane is not a reflection of stellar evolution but rather a reflection of the composition of the material from which the stars were formed. Thus, as previously stated, the plot of [α/Fe] versus [Fe/H] is a stellar population diagram that together with some age dimension may externalize signatures of stellar populations from different epochs of the Milky Way.

In order to identify and delimit these two sequences, we use hypothesis tests to characterize which values of [α/Fe] along [Fe/H] segregate these two disc populations by $v \sin i$ measures, that is, reject the null hypothesis that both samples are drawn from the population with a confidence level of 95 per cent. In the application of these tests we disregard stars with small surface convection zones since their shallow convective envelopes inhibit the generation of a strong magnetic field and the angular momentum loss, hence reducing the rotation-age relationship on the main sequence. To do this, we analysed a more homogeneous sample of stars with surface temperatures $T_{\rm eff} < 6200$ K (roughly $M < 1.3\,M_{\odot}$). This temperature threshold is often called 'Kraft break' (Kraft 1967; Van Saders & Pinsonneault 2013; Becker et al. 2017), corresponding to stellar configurations where the convective outer envelope becomes thin or radiative for effective temperatures higher than 6200 K (Marsh et al. 2017). The resulting subsample is composed of 2730 stars mostly of G-types with effective temperatures $5400 < T_{\rm eff} < 6200$ K and $v \sin i$ up to 9 km s^{-1} (~ 96 per cent).

The hypothesis tests consist of applying a two-sample Anderson–Darling (AD) test[1] for age proxy, $v \sin i$, at different adjacent intervals along [α/Fe] – for each region of [Fe/H]. The A^2_{nm} statistic of the AD test is

$$A^2_{nm} = \frac{nm}{n+m} \int_{-\infty}^{\infty} \frac{[F_n(x) - G_m(x)]^2}{H_{n+m}(x)[1 - H_{n+m}(x)]} {\rm d}H_{n+m}(x), \quad (1)$$

where

$$F_n(x) = \begin{cases} 0, & \text{if } x < x_{(1)} \\ i/n, & \text{if } x_{(i)} \leq x < x_{(i+1)}, i = 1, 2, ..., n-1 \\ 1 & \text{if } x \geq x_{(x)} \end{cases} \quad (2)$$

In the same way to $G_m(x)$, and

$$H_{n+m}(x) = [nF_n(x) + mG_m(x)](n+m). \quad (3)$$

[1]K-sample Anderson–Darling test from scipy anderson_ksamp.

n e m are the sizes of the samples, and $F_n(x)$ and $G_m(x)$ are the functions of empirical distributions of $v \sin i$, $x = v \sin i$, in two different adjacent regions of the [α/Fe]–[Fe/H] plane. The term $H_{n+m}(x)[1 - H_{n+m}(x)]$ in equation (1) is a weighting function that ensures the same statistical weight over the entire distribution of projected rotational velocities, making the AD test more sensitive, powerful, and therefore more advisable than other tests like, e.g. Kolmogorov–Smirnov and Cramer-von Mises, mainly when applied to stellar rotation velocities where the distributions are generally characterized by tails (at larger values of $v \sin i$).

Found the different regions of [α/Fe] with statistically distinct $F_n(x)$ and $G_m(x)$ distributions along [Fe/H] at intervals or steps of 0.02 and 0.04 dex, we compute the median of these results and perform a polynomial fit over metallicity

$$[\alpha/{\rm Fe}](\lambda) = \sum_{i=0}^{N} A_i \lambda^i, \quad (4)$$

where

$$\lambda = \frac{[{\rm Fe/H}]_0 + {\rm step}}{2}, \frac{([{\rm Fe/H}]_0 + {\rm step}) + {\rm step}}{2}, \ldots \quad (5)$$

To our sample $[{\rm Fe/H}]_0 = -1.0$ dex, with steps of 0.04 and 0.06 dex.

The adjacent intervals analysed in the [α/Fe] axis are constructed in pairs, taking into account different minimum amounts of 5, 10, 15,..., 30 stars and sweeping the [α/Fe] ratios in steps of 0.01, 0.02, 0.03, 0.04, and 0.05 dex at a time.[2] This ensures robustness in the analysis (30 iterations for each [Fe/H] region), since different initial amounts of stars result in slightly different outputs, which is also equally true for the steps. The left panel in Fig. 2 illustrates part of this approach of identifying regions with different rotation distributions along the metallicity in steps of 0.06 dex. The curve determined by projected rotational velocities from cold star subsample (defined by

[2]For example, in a given region of [Fe/H], we sweep the [α/Fe] axis from 0.01 to 0.01 dex looking for two neighbouring intervals with at least 5 stars in each. After identifying the two intervals, we used the AD test to determine whether these two regions contain stellar rotation values corresponding to distinct populations with a 95 per cent confidence level. Sweeping the entire [α/Fe] axis for each [Fe/H] range, we repeat the same procedure, for the same step of 0.01 dex, now considering neighbouring intervals that contain at least 10 stars and so on for 15, 20, 25, and 30 stars. This procedure is repeated with different initial steps of 0.02, 0.03, 0.04, and 0.05 dex.

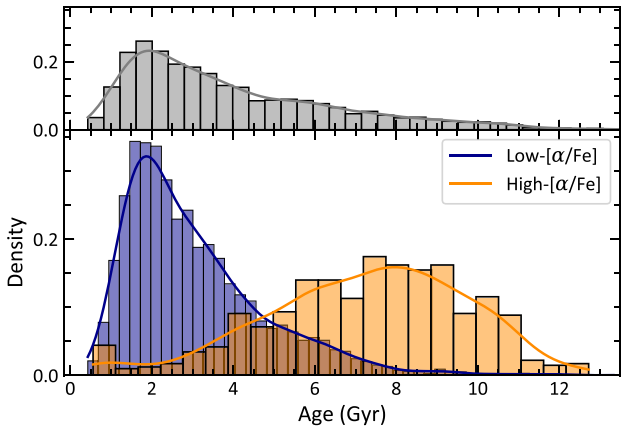

Figure 3. Age histogram for the high- and low-[α/Fe] sequences. The upper plot shows the total data set combined. The number of bins and the bandwidth of the kernel density estimate were determined using Silverman's rule.

Kraft-break) is

$$[\alpha/\mathrm{Fe}] = 0.012 - 0.473[\mathrm{Fe/H}] + 0.295[\mathrm{Fe/H}]^2 + 0.614[\mathrm{Fe/H}]^3 \quad (6)$$

4 RESULTS

Fig. 2 shows the polynomial fit curve, equation (6), plotted to our initial sample of F- and G-type stars and the two rotation-chemical disc populations disentangled. The resulting populations comprise 737 stars attributed to *high*-[α/Fe] component (stars above the curve) and 3836 stars attributed to *low*-[α/Fe] component (stars below the curve). The age distribution of these two branches of stars is shown in Figs 3 and 4. Noticeably the two disc components are significantly different: the high-[α/Fe] sequence is composed of mainly older ($\sim$12–6 Gyr), but also contains young stars with a wide range of ages, whereas the low-[α/Fe] population is dominated by stars 2 Gyr old and intermediate ages extending to 7 Gyr. The median ages of the low- and high-[α/Fe] stars are respectively 2.6 and 7.5 Gyr, and a boundary age–age at which 80 per cent of the stars are either above or below this value or simply the shared age at which it has a low number of stars – around 5 Gyr.

Such double sequences of age and its feature distributions are consistent with the widely suggested high- and low-α sequences or chemically defined 'thin disc' and 'thick disc' components in spectroscopic studies of Solar neighbourhood (Haywood et al. 2013; Xiang et al. 2017; Mackereth et al. 2019a; Lagarde et al. 2021) and mainly in simulation studies (see Brook et al. 2012; Grand et al. 2017; Clarke et al. 2019; Vincenzo & Kobayashi 2020; Yu et al. 2021). For instance, Lagarde et al. (2021) using the APOKASC sample (APOGEE survey+*Kepler* mission) of evolved stars that extends up to 4 kpc, with ages determined from asteroseismology, showed age distributions very close to those we found, which also reveal two distinct age peaks around 1–2 and 7–8 Gyr to their thin and thick disc populations, respectively.

It is worth noting that due to cutoff imposed at the effective temperature (>5400 K), which favours the observation of younger stars, and the selection effect on GCS data that is made up of bright stars and limited near the disc plane, leads again to a net bias against old objects, the age distribution of the high- land low-[α/Fe] sequences is shifted towards lower age values, with a strong peak around 2 Gyr for [α/Fe] stars. Furthermore, as the central region

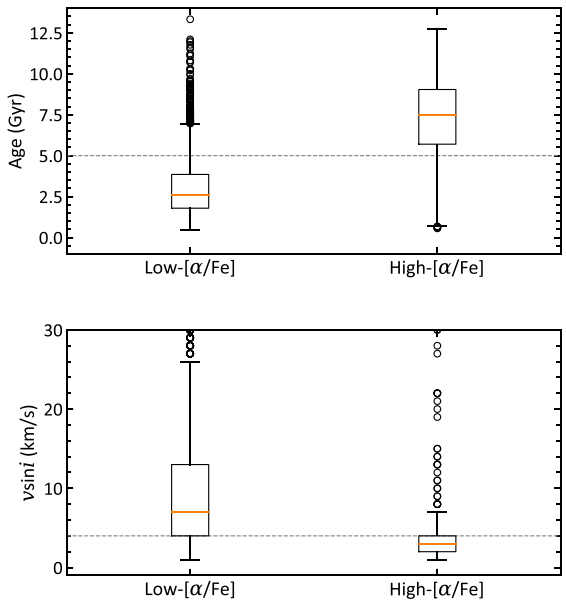

Figure 4. Boxplots for age (top) and $v \sin i$ distributions (bottom) of both high and low [α/Fe] sequences. The dotted lines at 5 Gyr and 4 km s^{-1} in the two plots correspond to 80 per cent of each component.

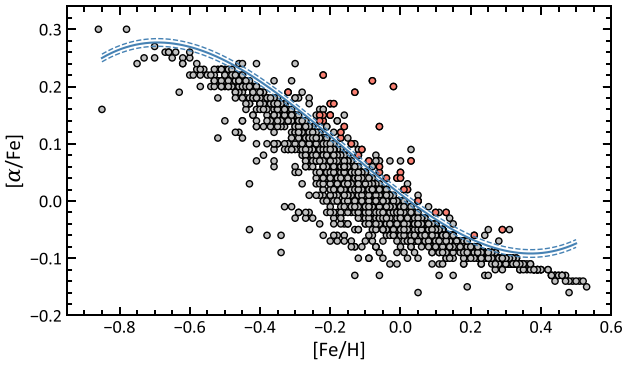

Figure 5. The [α/Fe]–[Fe/H] plane for stars with projected rotational velocity $>$ 4 km s^{-1}. The red dots represent young stars (<5 Gyr) in the high-[α/Fe] region.

of the [α/Fe] versus [Fe/H] diagram is characterized by a strong overlap of young and old stars (fast and slow rotors), if we analysed the rotational behaviour of the initial sample of FG stars without applying the stellar effective temperature limit below the Kraft break, most of which are hot and hence with a weak age-rotation relationship ($T_{\rm eff} > 6200$ K), the result of the split in the chemical diagram would possibly be biased towards the low region of young stars. The fraction of high/low-[α/Fe] stars for our disentangled disc populations is 737/3836 $\sim$ 0.19, which is consistent within the range of estimates of the local density ratio of the thick/thin disc stars, 2 per cent to 15 per cent (Gilmore & Reid 1983; Soubiran, Bienaymé & Siebert 2003; Jurić et al. 2008; De Jong et al. 2010). Based on separation in velocity-metallicity space, Soubiran, Bienaymé & Siebert (2003) estimated a fraction of 15 $\pm$ 7 per cent for thick disk and 85 $\pm$ 7 per cent for thin disc stars in the local 400 pc sample. Similarly, Anguiano et al. (2020), from the APOGEE DR16 and Gaia DR2 surveys, found that 81.9 per cent of their data set are thin disc stars, and about 16.6 per cent of stars belong to the thick disc, with the

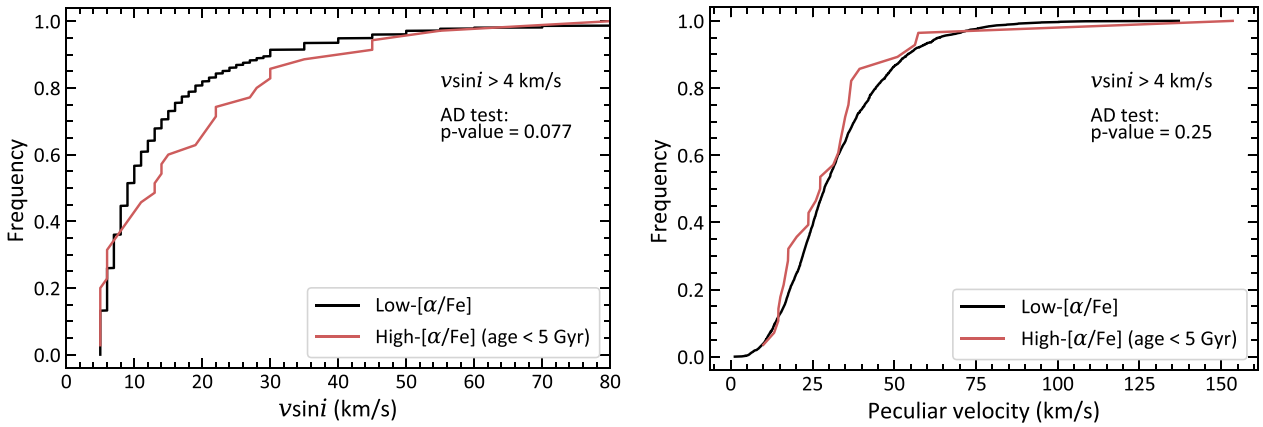

Figure 6. Cumulative distributions of projected rotational velocity (right) and peculiar velocity or total spatial velocity (left) for stars with rates > 4 km s^{-1}.

other 1.5 per cent of the objects belonging to the Milky Way stellar halo.

The $v \sin i$ distributions of the high- and low-sequences are shown in the lower plot of Fig. 4. As expected, just as we saw in age distribution, the projected rotational velocities of two population branches are also quite different, with median rotation rate of 3 and 7 km s^{-1} for high- and low-[α/Fe] stars, respectively. The distinction becomes more expressive when we analyse the separation value of the rotation rates. Excluding the stars in the overlap region, 97 per cent of the $\sim$ 3000 stars with rotation rates greater than 4 km s^{-1} belong to the low-[α/Fe] sequence and the other 3 per cent (in the high-[α/Fe] region) almost half younger than 5 Gyr which indicates that these stars are possibly of the same population, see Fig. 5. Indeed, as shown in the Fig. 6, analysing $v \sin i$ and peculiar velocity empirical cumulative distributions through test AD of the low-[α/Fe] sequence and star in the high-[α/Fe] region up to 5 Gyr old, both with restriction $v \sin i > 4$ km s^{-1}, we found that these stars are not from distinct populations (within a significance level of 95 per cent).

4.1 Kinematic properties

We recalculate the space-velocity components $U_{\rm LSR}$, $V_{\rm LSR}$, and $W_{\rm LSR}$ with respect to the local standard of rest (LSR) using the parallaxes, proper motions, and radial velocities of the second data release of the ESA-Gaia mission, Gaia DR2 (Gaia et al. 2018). In the Galactic cardinal directions, $U_{\rm LSR}$ points towards the Galactic centre, $V_{\rm LSR}$ is in the direction of the Galactic rotation, and $W_{\rm LSR}$ and positive $W_{\rm LSR}$ towards the north Galactic pole. The motion of the Sun relative to the LSR was adopted as $(U_\odot, V_\odot, W_\odot) = (11.10, 12.24, 7.25)$ km s^{-1} of Schönrich, Binney & Dehnen (2010). The distribution of stars in the Toomre diagram is shown in Fig. 7, the total spatial velocity or total kinetic energy is given by $V_{\rm TOTAL} \equiv (U^2_{\rm LSR} + V^2_{\rm LSR} + W^2_{\rm LSR})^{1/2}$. Stars belonging to the low-[α/Fe] component have mostly total velocity $V_{\rm TOTAL} < 70$ km s^{-1} ($\sim$ 90 per cent) and about 80 per cent with values less than 50 km s^{-1}, characteristic values of the thin disc population (e.g. Nissen 2004; Loebman et al. 2011; Bensby, Feltzing & Oey 2014). Although the low [α/Fe] component corresponds to 'kinematically cool' stars, the high [α/Fe] component has both 'hot' and 'cold' kinematic aspects. In general, these kinematic parameters are in agreement with those observed in the old age sequence or nominally thick disc stars (e.g. Adibekyan et al. 2013; Bensby, Feltzing & Oey 2014; Silva Aguirre et al. 2018).

When the velocities $U_{\rm LSR}$, $V_{\rm LSR}$, and $W_{\rm LSR}$ are analysed in conjunction with the [Fe/H], the kinematic properties of the high-[α/Fe] population become clearer as shown in the plot on the right side in Fig. 7. We see that these stars are kinematically cold as [Fe/H] increases and, on the other hand, the dispersion of space velocities decreases, although the stellar age is basically the same along [Fe/H]. This is a well expected characteristic of the asymmetric drift of thick disc stars, where as metallicity and spatial rotational velocity increase, the velocity dispersion decrease. Interestingly, for [Fe/H] ratios < -0.4 dex the total space velocity of the high-[α/Fe] is essentially $50 \leq V_{\rm TOTAL} \leq 180$ km s^{-1}, values relatively close to the canonical space velocity of the thick disc (see Nissen & Schuster 2008; Bensby, Feltzing & Oey 2014). Such behaviour can be the effect of dynamic processes such as radial migration (e.g. Sellwood & Binney 2002; Roškar et al. 2008; Schönrich & Binney 2009a, b), a consequence of this process is the correlation between azimuthal velocity V_ϕ (or Cartesian velocity component $V_{\rm LSR}$) and metallicity of the thin and thick discs, but of opposite signs. The radial migration model predicts negative correlation between rotational velocities V_ϕ and metallicity for thin disc and little[3] positive correlation for thick disc component (Loebman et al. 2011) due to radial scattering triggered by non-axissymmetric perturbations (e.g. spiral arms), in which the stars move inward or outward of their birth radii (migrating radially over significant distances). The Galactocentric cylindrical rotational velocity is computed as follows:

$$V_\phi = -(V_{\rm LSR} + V_{\rm rot})\frac{X_{\rm GC}}{R} + U_{\rm LSR}\frac{Y_{\rm GC}}{R}, \quad (7)$$

where $R = \sqrt{X^2_{\rm GC} + Y^2_{\rm GC}}$ is the planar radial coordinate and $V_{\rm rot} = 220$ km s^{-1} is the amplitude of the Galactic rotation towards $l = 90^\circ$ (IAU standard value). In the right-handed reference frame, with the X-axis pointing towards the Galactic centre, the Galactic-centred Cartesian coordinates $(X_{\rm GC}, Y_{\rm GC}, Z_{\rm GC})$ are:

$$\begin{aligned} X_{\rm GC} &= d\cos(b)\cos(l) - X_\odot \\ Y_{\rm GC} &= d\cos(b)\sin(l) \\ Z_{\rm GC} &= d\sin(b). \end{aligned} \quad (8)$$

In such a coordinate system, d is the stellar distance from the Sun, l and b are the Galactic longitude and latitude, and the Sun located

[3] A priori, as the older stars had more time to mix radially throughout the disc, the expected trend is consequently weaker.

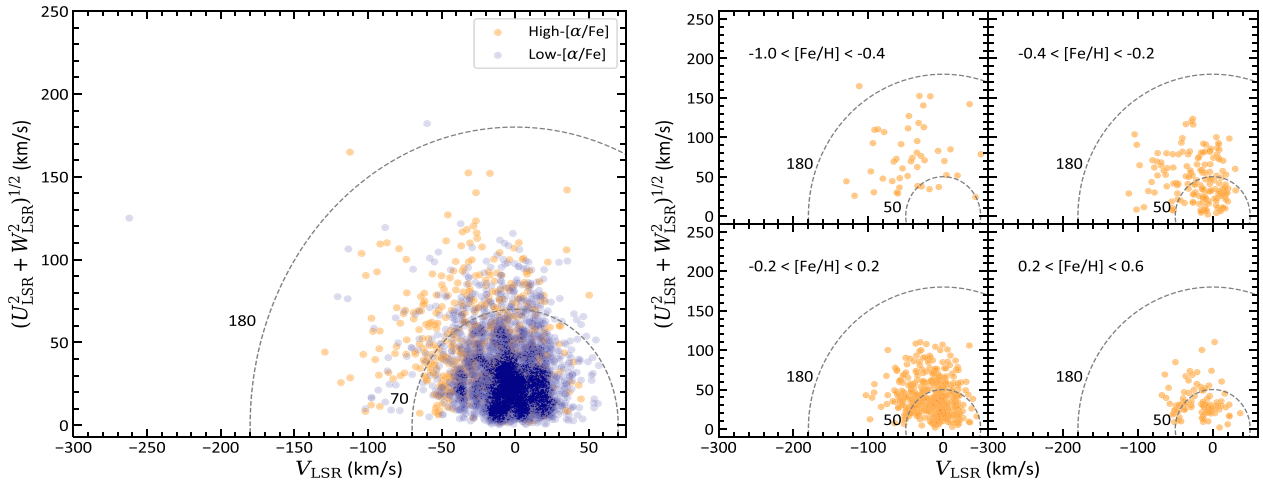

Figure 7. Left panel: Toomre diagram for two high- and low-[α/Fe] sequences. The dotted lines correspond to constant values of the total velocity. $V_{TOTAL} = (U^2_{LSR} + V^2_{LSR} + W^2_{LSR})^{1/2}$ of 70 and 180 km s^{-1}. The region V_{TOTAL} between 70 and 50 km s^{-1} is characterized as a probable zone of overlap or transition between the thin and thick disc components. Right panel: Toomre diagrams for high-[α/Fe] component in different intervals of [Fe/H].

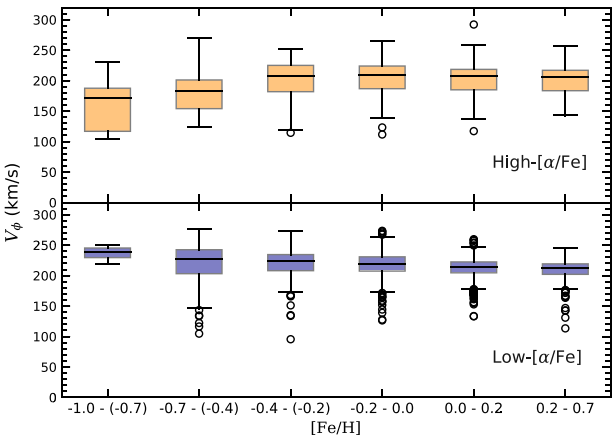

Figure 8. Boxplots of V_ϕ in different intervals of [Fe/H] for high- e low-[α/Fe] components.

at $(X_\odot, Y_\odot, Z_\odot) = (8.2, 0, 0.025)$ kpc (Bland-Hawthorn & Gerhard 2016). In Fig. 8 we have the azimuthal velocity V_ϕ as a function of metallicity for the two sequences high and low [α/Fe]. It is important to underline that in the first boxplot ($-1 <$ [Fe/H] < -0.7 dex) of the low-[α/Fe] sequence there are only three stars, making this region less representative, but this interval of metallicity reproduces the general behaviour expected of V_{LSR} with [Fe/H] and the stars are still significantly distinct from the high-[α/Fe] population stars.

For our two rotation-chemical disc components, we find a negative correlation in the spatial circular velocity V_{LSR} as a function of metallicity for low-[α/Fe] sequence, and for the high-[α/Fe] stars, in contrast, a positive gradient, $\partial V_\phi/\partial$[Fe/H] > 0, showing good agreement with the scenario of radial migration:

$$\frac{\partial V_\phi}{\partial[\mathrm{Fe/H}]} = -16.9 \pm 3.1 \text{ km s}^{-1}\,\text{dex}^{-1} \quad (\text{low} - [\alpha/\mathrm{Fe}]) \tag{9}$$

$$\frac{\partial V_\phi}{\partial[\mathrm{Fe/H}]} = +23 \pm 9.1 \text{ km s}^{-1}\,\text{dex}^{-1} \quad (\text{high} - [\alpha/\mathrm{Fe}]) \tag{10}$$

As the sample is limited to a volume of 120 pc, the velocity gradients, equations (9) and (10), are not directly influenced by the metallicity gradient in the Galaxy since the change in metallicity across this volume is small, ∂[Fe/H]$/\partial R \sim -0.07$ dex kpc^{-1} (e.g. Zhang, Chen & Zhao 2021). These results are astonishingly close to the values obtained by Prieto, Kawata & Cropper (2016) of $\partial V_\phi/\partial$[Fe/H] $= -18 \pm 2$ and $+23 \pm 10$ km s^{-1} dex^{-1} for nominally thin and thick disc components, respectively. Similar results also obtained from high- and medium-resolution surveys of FGK stars with ~ -17 km s^{-1} dex^{-1} (Adibekyan et al. 2013; Recio-Blanco et al. 2014; Yan et al. 2019) and -18.2 ± 2.3 km s^{-1} dex^{-1} (Peng et al. 2018) for thin disc stars. Although the velocity gradient as a function of metallicity of the high-[α/Fe] component is quite consistent with that of Prieto, Kawata & Cropper (2016), its slope is relatively shallower than other literature values. Nevertheless, when we exclude metal-rich stars applying the constraint of [Fe/H] < 0.1–0.15 dex we find a steep gradient of 42.1 to 47.6 km s^{-1} dex^{-1}, a result relatively close to the values found by different studies from 42 to 49 km s^{-1} dex^{-1} in Solar neighbourhood (Lee et al. 2011; Adibekyan et al. 2013; Recio-Blanco et al. 2014; Guiglion et al. 2015; Peng et al. 2018; Re Fiorentin, Lattanzi & Spagna 2019).

Given that we are considering an observable that is strongly influenced by the randomness of the rotational axes and a proxy variable of [α/Fe] abundance ratios, it is remarkable that the measurements of $v \sin i$ when applied on the chemical plane reproduce the ages and kinematic properties of disc components.

5 SUMMARY AND CONCLUSIONS

In this paper, we present a new approach to classifying Galactic disc populations by combining gyro- and chemochronology principles for dwarf stars of spectral types F and G in the Solar neighbourhood. Based on the assumption that the Galactic disc components are from different epochs and that this distinction, as well as their evolution, is externalized in the relationship between age and chemical abundances, we have focused on the disentangling of stellar populations relying on the behaviour of projected rotational velocity distributions in rotation–[α/Fe]–[Fe/H] space.

We select a sample of 5129 F- and G-type single stars from the GCS catalogue (Nordström et al. 2004; Holmberg, Nordström & Andersen 2007, 2009) with broad measures of $v \sin i$, estimates of proxy [α/Fe] abundance ratios, and revised astrophysical parameters

(Casagrande et al. 2011), comprising a cross-match with the second *Gaia* data release, Gaia DR2 (Gaia et al. 2018), that gives us an unparalleled data base of stars with 6D phase space information (full six-dimensional position and kinematic measurements). Our results show that the projected rotational velocity, despite its random nature of rotational axes, when used in conjunction with the [Fe/H] and [α/Fe] abundance ratios, is a great indicator of age and can be used in the segregation of stellar populations of the Galactic disc, establishing a characteristic value of $v \sin i$ where 98 per cent of the dwarfs with rotation rates > 4 km s^{-1} are of the low-[α/Fe] branch. With regard to age distributions, the high-[α/Fe] component is primarily formed of old stars ($\sim$ 12–6 Gyr) with a median age of about 7.5 Gyr but with an extended star formation for many Gyr, whereas the low-[α/Fe] sequence peaking at 2 Gyr with a median age of 2.6 Gyr.

Concerning the kinematics, the properties of the two sequences show good agreement with canonical components of the Galactic disc. We find cool, thin-disc-like kinematics in the low-[α/Fe] branch and hotter kinematics, among other thick-disc features, for the majority of the high-[α/Fe] stars. In addition, the asymmetric drift and dispersion of the space-velocity components ($U_{\rm LSR}$, $V_{\rm LSR}$, $W_{\rm LSR}$) decrease progressively along the high-[α/Fe] sequence as the metallicity increases. Our separation in the chemical rotational plane confirms the opposite correlations already observed of spatial rotational velocities, V_ϕ, and metallicity, [Fe/H], between the two Galactic disc populations in spectroscopic studies: we observe a positive gradient in the Galactic rotation as a function of metallicity of $\partial V_\phi/\partial$[Fe/H] $= +23 \pm 9$ km s^{-1} dex^{-1} for high-[α/Fe] component, which agrees with some studies (Loebman et al. 2011; Prieto, Kawata & Cropper 2016) but shallower than other literature values (e.g. Guiglion et al. 2015; Peng et al. 2018; Re Fiorentin, Lattanzi & Spagna 2019); for the low-[α/Fe] sequence, we find a negative trend in the spatial rotation velocities with metallicity, $\partial V_\phi/\partial$[Fe/H] $= -16.9 \pm 3.1$ km s^{-1} dex^{-1}, which is in very good agreement with several results from both medium- and high-resolution surveys of stars FGK in the Solar neighbourhood.

Regardless of the absence of any gap or apparent bimodality in the chemical distribution and inherent limitations in proxy measurements of α-elements, thanks to rotational rate analysis in rotation-chemical space in conjunction with the application of the stellar effective temperature limit below the Kraft break ($T_{\rm eff} < 6200$ K), we dissect the chemical and kinematic patterns as well as stellar properties of the Milky Way disc populations hidden on the [α/Fe]–[Fe/H] plot. The rotational-chemical sequences determined here, high- and low-[α/Fe] components, present different properties (enhanced [α/Fe] ratios, ages, kinematics, rotational lag, space velocity gradients, local density ratio) closely linked to stars of the chemically and kinematically defined thin and thick disc components in observational surveys (Recio-Blanco et al. 2014; Xiang et al. 2017; Silva Aguirre et al. 2018; Lagarde et al. 2021) and are broadly consistent with numerical simulations of Milky Way-like galaxies (Brook et al. 2012; Clarke et al. 2019; Vincenzo & Kobayashi 2020; Yu et al. 2021).

ACKNOWLEDGEMENTS

This work has made use of data from the European Space Agency (ESA) mission Gaia (https://www.cosmos.esa.int).

DATA AVAILABILITY

The stellar data used in this study are available through the Gaia archive facility at ESA (https://gea.esac.esa.int/archive/) and the Geneva–Copenhagen survey re-analysis database at http://vizier.cds.unistra.fr/viz-bin/VizieR-3?-source=J/A%2bA/530/A138. The data underlying this article will be shared on reasonable request to the corresponding author.

REFERENCES

Adibekyan V. Z., Santos N. C., Sousa S. G., Israelian G., 2011, A&A, 535, L11
Adibekyan V. Z. et al., 2013, A&A, 554, A44
Anguiano B. et al., 2020, AJ, 160, 43
Barnes S. A., 2003, ApJ, 586, 464
Becker J. C., Vanderburg A., Adams F. C., Khain T., Bryan M., 2017, AJ, 154, 230
Bensby T., Feltzing S., Lundström I., 2003, A&A, 410, 527
Bensby T., Feltzing S., Oey M., 2014, A&A, 562, A71
Bland-Hawthorn J., Gerhard O., 2016, ARA&A, 54, 529
Bovy J., Rix H.-W., Hogg D. W., 2012, ApJ, 751, 131
Brook C. B. et al., 2012, MNRAS, 426, 690
Buder S. et al., 2019, A&A, 624, A19
Casagrande L., Schönrich R., Asplund M., Cassisi S., Ramirez I., Melendez J., Bensby T., Feltzing S., 2011, A&A, 530, A138
Clarke A. J. et al., 2019, MNRAS, 484, 3476
De Jong J. T., Yanny B., Rix H.-W., Dolphin A. E., Martin N. F., Beers T. C., 2010, ApJ, 714, 663
Franchini M. et al., 2020, ApJ, 888, 55
Fuhrmann K., 1998, A&A, 338, 161
Gaia C. et al., 2018, A&A, 616
Gilmore G., Reid N., 1983, MNRAS, 202, 1025
Grand R. J. J. et al., 2017, MNRAS, 474, 3629
Gratton R. G., Carretta E., Matteucci F., Sneden C., 2000, A&A, 358, 671
Guiglion G. et al., 2015, A&A, 583, A91
Haywood M., Matteo P. D., Lehnert M. D., Katz D., Gómez A., 2013, A&A, 560, A109
Haywood M., Lehnert M. D., Matteo P. D., Snaith O., Schultheis M., Katz D., Gómez A., 2016, A&A, 589, A66
Ho A. Y., Rix H.-W., Ness M. K., Hogg D. W., Liu C., Ting Y.-S., 2017, ApJ, 841, 40
Holmberg J., Nordström B., Andersen J., 2007, A&A, 475, 519
Holmberg J., Nordström B., Andersen J., 2009, A&A, 501, 941
Jurić M. et al., 2008, ApJ, 673, 864
Kawaler S. D., 1988, ApJ, 333, 236
Kobayashi C., Taylor P., 2023, Handbook of Nuclear Physics. Springer, Berlin
Kraft R. P., 1967, ApJ, 150, 551
Lagarde N. et al., 2021, A&A, 654, A13
Lee Y. S. et al., 2011, ApJ, 738, 187
Loebman S. R. et al., 2011, ApJ, 737, 8
Mackereth J. T. et al., 2019a, MNRAS, 482, 3426
Mackereth J. T. et al., 2019b, MNRAS, 489, 176
Marsh F., Prince T., Mahabal A., Bellm E., Drake A., Djorgovski S., 2017, MNRAS, 465, 4678
de Medeiros J. R., Mayor M., 1999, A&AS, 139, 433
Minchev I., Chiappini C., Martig M., 2013, A&A, 558, A9
Navarro J. F., Abadi M. G., Venn K. A., Freeman K. C., Anguiano B., 2011, MNRAS, 412, 1203
Nissen P. E., 2004, in McWilliam A., Rauch M., eds, Origin and Evolution of the Elements. Cambridge Univ. Press, Cambridge, p. 154
Nissen P. E., Schuster W. J., 2008, in Andersen J., Bland-Hawthorn J., Nordström B., eds, Proc. IAU Symp. 254, the Galaxy Disk in Cosmological Context. Cambridge Univ. Press, Cambridge, p. 103
Nordström B. et al., 2004, A&A, 418, 989
Peng X., Wu Z., Qi Z., Du C., Ma J., Zhou X., Jia Y., Wang S., 2018, PASP, 130, 074102
Prieto C. A., Kawata D., Cropper M., 2016, A&A, 596, A98
Prochaska J. X., Naumov S. O., Carney B. W., McWilliam A., Wolfe A. M., 2000, AJ, 120, 2513
Queiroz A. B. A. et al., 2023, A&A, 673, A155

Re Fiorentin P., Lattanzi M. G., Spagna A., 2019, MNRAS, 484, L69
Recio-Blanco A. et al., 2014, A&A, 567, A5
Roškar R., Debattista V. P., Quinn T. R., Stinson G. S., Wadsley J., 2008, ApJ, 684, L79
Schönrich R., Binney J., 2009a, MNRAS, 396, 203
Schönrich R., Binney J., 2009b, MNRAS, 399, 1145
Schönrich R., Binney J., Dehnen W., 2010, MNRAS, 403, 1829
Sellwood J. A., Binney J., 2002, MNRAS, 336, 785
Silva Aguirre V. et al., 2018, MNRAS, 475, 5487
Skumanich A., 1972, ApJ, 171, 565
Soderblom D. R., 1983, ApJS, 53, 1
Soubiran C., Bienaymé O., Siebert A., 2003, A&A, 398, 141
Spitzer Lyman J., Schwarzschild M., 1951, ApJ, 114, 385
Spitzer Lyman J., Schwarzschild M., 1953, ApJ, 118, 106
Van Saders J. L., Pinsonneault M. H., 2013, AJ, 776, 67
Vincenzo F., Kobayashi C., 2020, MNRAS, 496, 80
Wojno J. et al., 2016, MNRAS, 461, 4246
Xiang M. et al., 2017, ApJS, 232, 2
Yan Y., Du C., Liu S., Li H., Shi J., Chen Y., Ma J., Wu Z., 2019, ApJ, 880, 36
Yu S. et al., 2021, MNRAS, 505, 889
Zhang H., Chen Y., Zhao G., 2021, ApJ, 919, 52

This paper has been typeset from a TEX/LATEX file prepared by the author.